A complete disclosure of the hidden type-1 AGN in NGC 1068 thanks to 52 yr of broad-band polarimetric observation

F. Marin

Monthly Notices
of the
ROYAL ASTRONOMICAL SOCIETY

MNRAS **479,** 3142–3154 (2018)
Advance Access publication 2018 June 14

doi:10.1093/mnras/sty1566

A complete disclosure of the hidden type-1 AGN in NGC 1068 thanks to 52 yr of broad-band polarimetric observation

F. Marin★

Université de Strasbourg, CNRS, Observatoire Astronomique de Strasbourg, UMR 7550, F-67000 Strasbourg, France

Accepted 2018 June 8. Received 2018 June 7; in original form 2018 April 12

ABSTRACT

We create the first broad-band polarization spectrum of an active galactic nucleus (AGN) by compiling the 0.1–100 μm, 4.9, and 15 GHz continuum polarization of NGC 1068 from more than 50 yr of observations. Despite the diversity of instruments and apertures, the observed spectrum of linear continuum polarization has distinctive wavelength-dependent signatures that can be related to the AGN and host galaxy physics. The impact of the Big Blue bump and infrared bump, together with electron, Mie scattering, dichroism, and synchrotron emission are naturally highlighted in polarization, allowing us to reveal the type-1 AGN core inside this type-2 object with unprecedented precision. In order to isolate the AGN component, we reconstruct the spectral energy distribution of NGC 1068 and estimate the fraction of diluting light in the observed continuum flux. This allows us to clearly and independently show that, in the case of NGC 1068, Thomson scattering is the dominant mechanism for the polarization in the optical band. We also investigate the effect of aperture on the observed polarization and confirm previous findings on the extension of the narrow line region of NGC 1068 and on the *B*-band and *K*-band polarization from the host. Finally, we do not detect statistically significant aperture-corrected polarimetric variations over the last 52 yr, suggesting that the parsec-scale morphological and magnetic geometries probably remained stable for more than half a century.

Key words: polarization – catalogues – galaxies: active – galaxies: fundamental parameters – galaxies: nuclei – galaxies: Seyfert.

1 INTRODUCTION

NGC 1068, also commonly known as M77, is one of the most studied active galactic nuclei (AGNs). Its proximity to the Earth ($z = 0.003793$, $d^1 = 10.582^{+5.418}_{-3.402}$ Mpc) and its bolometric luminosity ($\sim 2 \times 10^{45}$ erg s^{-1}, Hönig, Prieto & Beckert 2008; Raban et al. 2009) make NGC 1068 an ideal target for spectroscopic, polarimetric, and high-resolution angular imaging studies. It allows high signal-to-noise ratio observation (e.g. Low & Rieke 1971; Wilson & Elvis 1997; Alexander, Young & Hough 1999; Bauer et al. 2015), which is imperative to distinguish the central AGN from its host spiral galaxy (Balick & Heckman 1985). It is an essential point as the properties of the intermediate region between the inner AGN dust material and the outer circumnuclear star-forming regions of NGC 1068 can probe in great details the co-evolution of the AGN and its host galaxy (Vollmer, Beckert & Davies 2008; Schartmann et al. 2009, 2010).

The AGN in NGC 1068 was the key-point of the Unified Model for radio-quiet objects[2] such as postulated by Antonucci (1993). This zeroth order geometrical scheme has proven to be particularly successful in explaining a large fraction of observational features in many radio-quiet AGN thanks to a critical point: the nuclear orientation of the central engine. Depending on the inclination of the observer with respect to the polar axis of the object, defined as the direction towards which the outflows of the AGN are directed, a variety of emission lines can be detected. Khachikian & Weedman (1974) defined two types of Seyferts galaxies. In their nomenclature, Seyfert-2s show narrow permitted and forbidden emission lines while Seyfert-1s show broad permitted emission lines in addition to the Seyfert-2s lines. The reason for the disappearance of the broad permitted emission lines in types-2s was a crucial question that was solved largely thanks to observations of NGC 1068.

★ E-mail: frederic.marin@astro.unistra.fr

[1]Redshift-independent distance computed by the NED from 11 distances in the literature.

[2]We acknowledge that the spectropolarimetric study of the radio galaxy 3C 234 preceded the work on NGC 1068, revealing a type-1 spectrum in polarized light together with a high-polarization degree oriented perpendicular to the radio axis (Antonucci 1982, 1984). However, 3C 234 is a radio-loud AGN, while NGC 1068 is radio-quiet.

Antonucci & Miller (1985) have shown that high-resolution (5–10 Å), high signal-to-noise ratio polarization spectra of the nucleus of NGC 1068 are necessary to uncover broad Balmer lines and Fe II emission. Those lines have been found to have an intrinsic polarization >15 per cent at approximately the same position angle (PA) as that of the continuum, and their line wings appear broadened in the polarized flux spectra only. It was a definite set of proofs that a Seyfert-1 nucleus is hiding inside NGC 1068. The polarization angle, perpendicular to the axis of radio emission, is the strongest evidence for polar scattering of inner AGN photons, imprinting the polarized spectrum with the broad emission line. To explain the absence of broad lines in total flux and the orientation of the polarization angle, the most convenient way is to postulate the existence of a reservoir of circumnuclear dust that is enshrouding the nucleus along the equatorial plane. According to the inclination of the observer, the central engine can be directly observed (Seyfert-1s) or it is obscured by dust (Seyfert-2s). It naturally explains the disappearance of the broad permitted emission line that can only be detected in polarized flux. The theory was also confirmed in radio-loud AGN (Antonucci 1984; Barthel 1989), leading to a unification of radio-loud AGN that includes radio galaxies, quasars, and blazars (Urry & Padovani 1995).

Polarimetric observations of NGC 1068 had a significant impact on our global comprehension of AGN but many questions that can be solved with polarimetry remain open. The systematic search for hidden type-1 cores in Seyfert-2s allows one to test whether all AGN are fundamentally the same in terms of physical components. Optical spectropolarimetry revealed broad components of Balmer lines in many type-2s but a fraction of them are reluctant to show broad permitted emission lines in their linearly polarized spectrum (see e.g. Young et al. 1995; Moran et al. 2000; Young 2000; Tran 2003; Ramos Almeida et al. 2016). New high resolution, high signal-to-noise ratio polarimetric observations of AGN on modern telescopes with large mirrors are necessary to test if some type-2 AGN genuinely lack a type-1 core. In addition, high angular resolution, high contrast polarimetric imaging using adaptive optics have shown that nearby bright AGN can be observed at phenomenal resolutions in the near-infrared (e.g. Gratadour et al. 2015; Lopez-Rodriguez et al. 2015). Gratadour et al. (2015) used the extreme adaptive optics system on the SPHERE instrument at the very large telescope to observe NGC 1068 in the H (1.65 μm) and K' (2.2 μm) bands, and achieved polarimetric images with resolution 0.068 arcsec (∼4 pc at $d \approx 14$ Mpc, which is the distance usually chosen for this object). By doing so, the authors revealed a compact elongated[3] (20 × 60 pc) structure, tracing the scattering regions at the center of NGC 1068, together with the already seen hourglass-shaped polar winds (see e.g. Capetti et al. 1995a,b; Kishimoto 1999). The later author pushed the polarimetric study of the ultraviolet linear polarization of the polar outflows up to the determination of the location of the nucleus of NGC 1068 and figured out the three-dimensional structure of its winds.

There is a lot more to be discovered by polarimetry. One can test the geometry of the region responsible for the emission of the broad permitted line (Smith et al. 2002). It should be possible to determine the spin, mass, and inclination of the central supermassive black hole thanks to X-ray polarimetry (Dovčiak, Karas & Matt 2004; Schnittman & Krolik 2009, 2010; Dovčiak et al. 2011). The composition and location of almost all the AGN components can be probed independently of the fact that they are obscured by dust or gas. Even the presence of aborted jets may be detected. To reach this goal, broad-band polarimetry is needed. Ramos Almeida et al. (2016) have clearly showed that information can be missed if we focus on a too narrow waveband. But is there enough published data to test the Unified Model of AGN at all wavebands? Do we need further instruments on large class telescopes? What is the broad-band continuum polarization spectrum of radio-quiet AGN and what are the wavebands to be still explored?

To answer those questions, we present a thorough compilation of all the continuum polarimetric observations of NGC 1068 in order to create, for the first time, a combined spectrum of the linear polarization of an archetypal type-2 AGN. We use the fact that no other AGN have as much published polarimetric data as NGC 1068 to estimate the impact of several observational constraints on the detected polarization levels. We also investigate the time evolution of polarization over ∼52 yr and check whether NGC 1068 has evolved in terms of geometry. By doing so we aim at making a strong case for future polarimetric instruments and programmes. In this paper, we compile the published polarimetric data on NGC 1068 in Section 2.1 and build the combined polarized spectrum of NGC 1068 in Section 2.2. We investigate the effect of apertures in Section 2.3 before computing the global spectral energy distribution (SED) of the system in Section 2.4. We use this multicomponent SED to correct the continuum polarization from starlight dilution in Section 2.5 and demonstrate the predominance of electron scattering. Finally, we examine the temporal evolution of the linear polarization of NGC 1068 in Section 2.6. We discuss our results and the important observations to be made in the future in Section 3 before concluding our paper in Section 4.

2 THE DATA

To gather the polarimetric observations published in refereed papers, the SAO/NASA Astrophysics Data System (ADS) was extensively used. The SAO/NASA ADS is a Digital Library portal for researchers in Astronomy and Physics, operated by the Smithsonian Astrophysical Observatory (SAO) under a NASA grant; its website is accessible here: http://adsabs.harvard.edu/. Keywords and filtering by object name (NGC 1068 and its alternative names) allowed for easier detection of relevant papers. Discussions with experts in the field, acknowledged at the end of this paper, also helped to find obscure publications. Several journal were also contacted to retrieve non-indexed results mentioned in several publications (Astronomical Journal, Astronomical Circular).

2.1 The catalogue

The final catalogue of polarimetric[4] observations of NGC 1068 is presented in Table 1. It contains 34 publications spanning over more than 50 yr (1965–2017, observational dates, not paper publication

[3] Atacama Large Millimeter/sub-millimeter Array (ALMA) observations have revealed that the torus has an extension of ∼5×10 pc at 432 μm (Gallimore et al. 2016; García-Burillo et al. 2016; Imanishi et al. 2018). The structure suggested by Gratadour et al. (2015) should be taken as an upper limit due to the methodology used by the authors.

[4] We focus on NGC 1068 linear polarization. Circular polarization, at least in the near-ultraviolet, optical and near-infrared bands, has been the subject of an unsolved debate. One paper claimed a non-detection (Landstreet & Angel 1972), another a non-significant detection (Gehrels 1972), and two others a clear detection (Nikulin, Kuvshinov & Severny 1971; Angel et al. 1976).

Table 1. Catalogue of published polarimetric measurements of NGC 1068. The first column is the reference paper, the second column is the instrument used for the measurement, the third column is the waveband or filters used during the observation, the fourth column is the observation aperture (in arcseconds), and the fifth column indicates if polarimetric images were taken.

Reference	Instrument	Waveband	Aperture	Imaging
Dibai & Shakhovskoi (1966)	Integrating electropolarimeter of the Crimean Astrophysical Observatory	*U*, *B*, *V* filters	15 arcsec, 25 arcsec	
Dombrovskii & Gagen-Torn (1968)	Electropolarimeter of Leningrad University	*U*, *B*, *V*, *R* system, ZhS-18, and SZS-22 filters	13 arcsec, 26 arcsec	
Kruszewski (1968)	Catalina 154-cm Telescope	*U* (2.78 μm^{-1}), *H* (2.33), *G* (1.93), *O* (1.56), *R* (1.21), and *I* (1.06)	9.2 arcsec, 10.2 arcsec	
Visvanathan & Oke (1968)	60- and 100-in. telescopes at Mount Wilson	*U*, *B*, *V*, *R* system	12.5 arcsec, 19.0 arcsec, 28.0 arcsec	
Kruszewski (1971)	Catalina 154-cm Telescope	*U* (2.78 μm^{-1}), *H* (2.33), *G* (1.93), *O* (1.56), *R* (1.21), and *I* (1.06)	6.8 arcsec, 9.2 arcsec, 10.2 arcsec, 15 arcsec, 30.6 arcsec	
Knacke & Capps (1974)	1.3-m telescope of the Kitt Peak National Observatory	3.5 μm ($\Delta\lambda = 0.6$ μm), 10.2 μm ($\Delta\lambda = 6$ μm), and 18.4 μm ($\Delta\lambda = 1$ μm)	12 arcsec	
Angel et al. (1976)	90-in. (2.3 m) telescope of Steward Observatory	3200–8600 Å	2 arcsec	
Dyck & Jones (1976)	Unknown	1.2 μm, 2.2 μm	5.4 arcsec, 11 arcsec	
Elvius (1978)	72-in. Perkins Telescope of the Ohio Wesleyan Observatory	Schott UG1 filter	13 arcsec-long slit	
Lebofsky, Kemp & Rieke (1978)	Steward Observatory 90-in. telescope	*J*, *H*, *K*, *L′* filters	4 arcsec, 6 arcsec, 8 arcsec	
Wilson & Ulvestad (1982)	Very Large Array	15 GHz	0.7 arcsec	✓
Martin et al. (1983)	Steward Observatory 2.3-m, Las Campanas 1.0- and 2.5-m, Kitt Peak 1.3- and 2.1-m, and University of Western Ontario 1.2-m telescopes	C500 filter (blue–green)	5 arcsec	
McLean et al. (1983)	3.9-m Anglo-Australian Telescope	3900–8000 Å	1.7 arcsec × 2.2 arcsec, 2 arcsec × 2.5 arcsec	
Miller & Antonucci (1983)	Lick 3-m Shane Telescope	3500–5300 Å	2.8 arcsec	
Wilson & Ulvestad (1983)	Very Large Array	4.9 GHz	1 arcsec	✓
Aitken et al. (1984)	3.9-m Anglo-Australian Telescope and 3.0-m Infrared Telescope in Hawaii	8–13.1 μm	4.2 arcsec, 5.6 arcsec, 15 arcsec, 50 arcsec	
Antonucci & Miller (1985)	Lick 3-m Shane Telescope Image Dissector Scanner	3500–7000 Å	2.8 arcsec	
Bailey et al. (1988)	3.9-m Anglo-Australian Telescope	0.36–4.8 μm	4.5 arcsec, 6.0 arcsec	
Scarrott et al. (1991)	3.9-m Anglo-Australian Telescope	*V*, *K* filters	1.6 arcsec, 2.8 arcsec, 4.5 arcsec	✓
Code et al. (1993)	Wisconsin Ultraviolet Photo-Polarimeter Experiment	1500–3200 Å	6 arcsec × 12 arcsec	
Antonucci et al. (1994)	*Hubble Space Telescope* Faint Object Spectrograph	1575–3300 Å	0.3 arcsec, 1 arcsec, 4.3 × 1.4 arcsec	
Capetti et al. (1995a)	*Hubble Space Telescope* Faint Object Camera and Wide Field Planetary Camera	2700–3700 Å, 5000–6000 Å	2.8 arcsec	✓
Capetti et al. (1995b)	*Hubble Space Telescope* COSTAR-corrected Faint Object Camera	2400–2700 Å	2.8 arcsec	✓
Tran (1995)	Lick 3-m Shane Telescope	4560–7355 Å, 4600–7400 Å, 3315–4400 Å	2.4 arcsec-slit	
Young et al. (1995)	3.8-m United Kingdom Infrared Telescope and the CGS4 spectrometer	0.46–0.77 μm, 1.18–1.38 μm, and 1.66–2.07 μm	3.08 × 3.0 arcsec	
Packham et al. (1997)	IR imaging polarimeter at the Anglo-Australian Telescope	*J*, *H*, K_n filters	2.0 arcsec, 4.5 arcsec, 6.0 arcsec	✓
Alexander et al. (1999)	United Kingdom Infrared Telescope, CGS4 spectrometer and IRPOL2	1.05–1.35 μm	1.23 arcsec × 6.7 arcsec	
Lumsden et al. (1999)	3.9-m Anglo-Australian Telescope	*J*, *H*, K_n, *N* filters	2.0 arcsec, 4.5 arcsec, 6.0 arcsec	✓
Simpson et al. (2002)	NICMOS Camera 2 on the *Hubble Space Telescope*	2 μm	3.0 arcsec	✓
Watanabe et al. (2003)	3.8 m United Kingdom Infrared Telescope	0.46–0.90 μm, 0.92–1.80 μm and 1.88–2.50 μm	3.5 arcsec	
Packham et al. (2007)	Gemini North 8.1-m telescope	9.7 μm	1.7 arcsec × 1.2 arcsec	✓
Mason et al. (2007)	IRPOL2 spectropolarimetry module and CGS4 on the 3.8m UK Infrared Telescope	3.10–3.67 μm	0.6 arcsec-slit	
Lopez-Rodriguez et al. (2015)	MMT-Pol on the 6.5-m MMT	*J′*, *K′* filters	0.2 arcsec, 0.5 arcsec, 2.0 arcsec	✓
Lopez-Rodriguez et al. (2016)	CanariCam on the 10.4-m Gran Telescopio CANARIAS	8.7 μm, 10.3 μm, 11.3 μm, 11.6 μm	0.4 arcsec, 2.0 arcsec	✓
Grosset et al. (in prep.)	SPHERE/VLT	*H* and *K′* bands	0.2 arcsec, 0.5 arcsec, 1.0 arcsec, 2.0 arcsec, 3.0 arcsec, 4.0 arcsec, 5.0 arcsec	✓
Lopez-Rodriguez et al. (in prep.)	HAWC+ on the 2.5-m SOFIA telescope	53 μm, 89 μm	5.0 arcsec, 8.0 arcsec	✓

timestamp). All papers are accounting for instrumental polarization, together with interstellar polarization. Due to the high Galactic latitude of NGC 1068 (−51.93°), Galactic contamination by diffuse interstellar grains is not expected to impact the measured polarization in the ultraviolet–far-infrared band (Prunet et al. 1998). However, a large fraction of authors did not corrected their data for dilution/contamination of the polarization by the host galaxy (exceptions include, but are not limited to, the work by Miller & Antonucci 1983; Antonucci & Miller 1985; Kishimoto 1999; Lopez-Rodriguez et al. 2015). The dust lane and host galaxy have a visual extinction $A_V \sim 9$ mag to the core of NGC 1068, producing an aperture-dependent level of dilution to be corrected at ultraviolet, optical, and infrared wavelengths. Unfortunately, this correction was not achieved by all the authors. To have a consistent set of measurements, the polarized values extracted from the aforementioned papers are the one that were not corrected for starlight dilution (but see Section 2.4 for the correction of polarization by removing the host component). The measurements were taken with a variety of instruments, listed in the second column of Table 1. Observations were made in different wavebands, from the ultraviolet using the Wisconsin Ultraviolet Photo-Polarimeter Experiment (Code et al. 1993) to the far-infrared using the SOFIA High-resolution

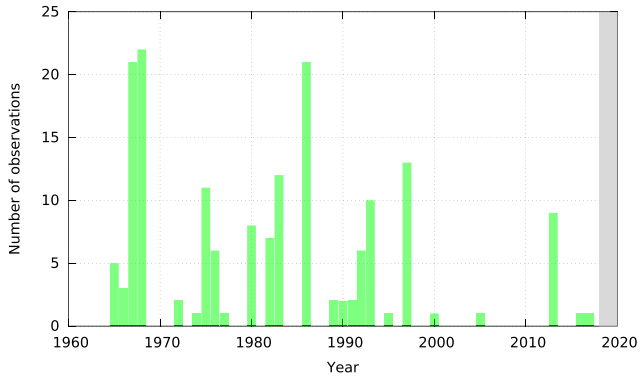

Figure 1. Number of observations per year dedicated to measure the broad-band continuum polarization of NGC 1068. The shaded area corresponds to the forthcoming years 2019–2020.

Airborne Wideband Camera-plus (HAWC+, Lopez-Rodriguez, E., private communication). Only two polarimetric observations have been published in the radio band, an upper limit at 15 GHz (Wilson & Ulvestad 1982) and a debated measurement at 4.9 GHz (Wilson & Ulvestad 1983). The bulk of observations was taken in the optical and near-infrared bands since they remain the easiest bands for ground observations. A variety of slits and circular apertures were used, depending on the technology available at that time (fourth column of Table 1). Finally, we have identified observations that were achieved in imaging modes. For these cases, the authors had polarization maps and could have, in principle, varied the aperture to remove the contribution of the host galaxy.

In Fig. 1, we present the temporal distribution of the number of polarimetric observations listed in our catalogue. The very first polarimetric observation of NGC 1068 listed in our sample goes back to 1965–1966 (Dibai & Shakhovskoi 1966). A year later, Dombrovskii & Gagen-Torn (1968) quoted polarimetric observations 'with a somewhat smaller aperture than ours' that might also have been achieved by Merle F. Walker in 1964 but the references listed in Dombrovskii & Gagen-Torn (1968) point towards papers that either are about other galaxies (M33, Walker 1964) or do not exist at all. A similar reference to the work by Walker (1964, p. 682) is mentioned in Elvius & Hall (1965) but the related paper could not be found. Hence, while we acknowledge that earlier polarimetric observations might have been achieved, we start our catalogue in 1965–1966 due to the lack of open-access publications.

The interest of the community for the polarimetric signature of NGC 1068 and similar galactic nuclei grew fast, with more than 50 observations achieved before 1970. The goal was to explore the origin of the observed polarization. Synchrotron emission was one of the two mechanisms (together with scattering) suggested to explain the high ultraviolet polarization in its nucleus (Elvius & Hall 1965). A few additional polarimetric measurements of this AGN occurred until the advent of the 3.9-m Anglo-Australian Telescope and the Lick 3-m Shane Telescope, which gave a new kick to observations in 1983 thanks to their large mirrors and up-to-date polarimeters. The true scattered polarization of NGC 1068 was estimated to be much higher than previously thought thanks to the careful removal of starlight from the host galaxy by Miller & Antonucci (1983). In addition, it was found that the PA of the optical continuum radiation is perpendicular to the axis of radio emission (18° ± 5, Wilson & Ulvestad 1982). After the breakthrough achieved in 1985, where Antonucci & Miller (1985) proved that a Seyfert-1 nucleus lies hidden in the core of NGC 1068, and that the origin of the continuum and broad-line polarization is due to scattering, the number of observations decreased. It was only in the mid of the 90s, when the Unified Model of AGN was synergized, confirmed and then reviewed (Antonucci 1993), that the community acquired a few more polarimetric observations of NGC 1068. Since the new millennium, only a dozen of polarimetric observations of this AGN have been achieved on 10-m class telescopes. Another observational gap could appear between the era of 10- and 30-m class telescopes, at least partly driven by the relative lack of polarimeters on such large telescopes.

2.2 Broad-band continuum polarization of NGC 1068

We compiled all the linear continuum polarization data of NGC 1068 in Fig. 2. When continuum polarization measurements were not estimated by the authors, we used WebPlotDigitizer to synthesize the polarization spectrum and extract the relevant numbers. WEBPLOTDIGITIZER (https://automeris.io/WebPlotDigitizer/) is a polyvalent and free software developed to facilitate easy and accurate data extraction from spectra, and it has already been used in Marin, Rohatgi & Charlot (2017) to reconstruct the ultraviolet spectropolarimetric spectrum of NGC 1068.

Our final spectrum spans from almost 0.1 to 100μm, together with two additional measurements at 4.9 and 15 GHz, with a variety of apertures, signal-to-noise ratios, and spectral resolutions. In this figure, we did not correct the polarization levels for the presence of diluting starlight emission originating from the host galaxy that may have a significant effect depending on the aperture of the observation/slit. This will be investigated in further details in Section 2.3. We plotted the continuum linear polarization in log scale to better contrast the fractional contribution of unpolarized light. The polarized flux is extracted from publications and is compared to a normal type-1 AGN total flux spectrum to investigate how the cross-section of the scatterer is changing with wavelength. The type-1 template we use was compiled by Prieto et al. (2010) and is the averaged SED of the high spatial resolution SEDs of NGC 3783, NGC 1566, and NGC 7469. The template was rescaled in order to be easily comparable to the polarized flux of NGC 1068. Finally, the polarization position angle (PPA) has been subtracted from the parsec-scale radio PA to check whether the polarization angle is parallel or perpendicular to the axis of the radio source associated with the galaxy (Antonucci 1993). We use the parsec-scale radio PA estimated by Wilson & Ulvestad (1982), but we acknowledge the fact that the PA is almost 0° at sub-arcesond scales (Muxlow et al. 1996). Our choice to use the parsec-scale value is coherent as the bulk of published polarimetric data having apertures larger than 1 arcsec.

We can see from Fig. 2 that the compiled polarization spectrum of NGC 1068 shows a coherent energy-dependent behaviour despite the multiple instruments, observational apertures, and observational dates. The linear continuum polarization is the highest in the ultraviolet band where starlight emission is weak: the starlight fluxes of spiral galaxies are about three orders of magnitude lower at 0.1μm than at 1 μm (Bolzonella, Miralles & Pelló 2000; Siebenmorgen & Krügel 2007). With increasing diluting fluxes from starlight, the continuum polarization of NGC 1068 decreases from ∼15 per cent at 0.1–0.2 μm to ∼1 per cent at 0.8–0.9 μm. The polarized flux, despite being not as well sampled as the polarization degree due to the lack of reported flux measurements, clearly shows the turnover of host dominance. At ultraviolet wavelengths, the polarized flux is constant while it decreases sharply in the optical, dipping at ∼1 μm. The dip in polarization at ∼1 μm is due to the maximum of

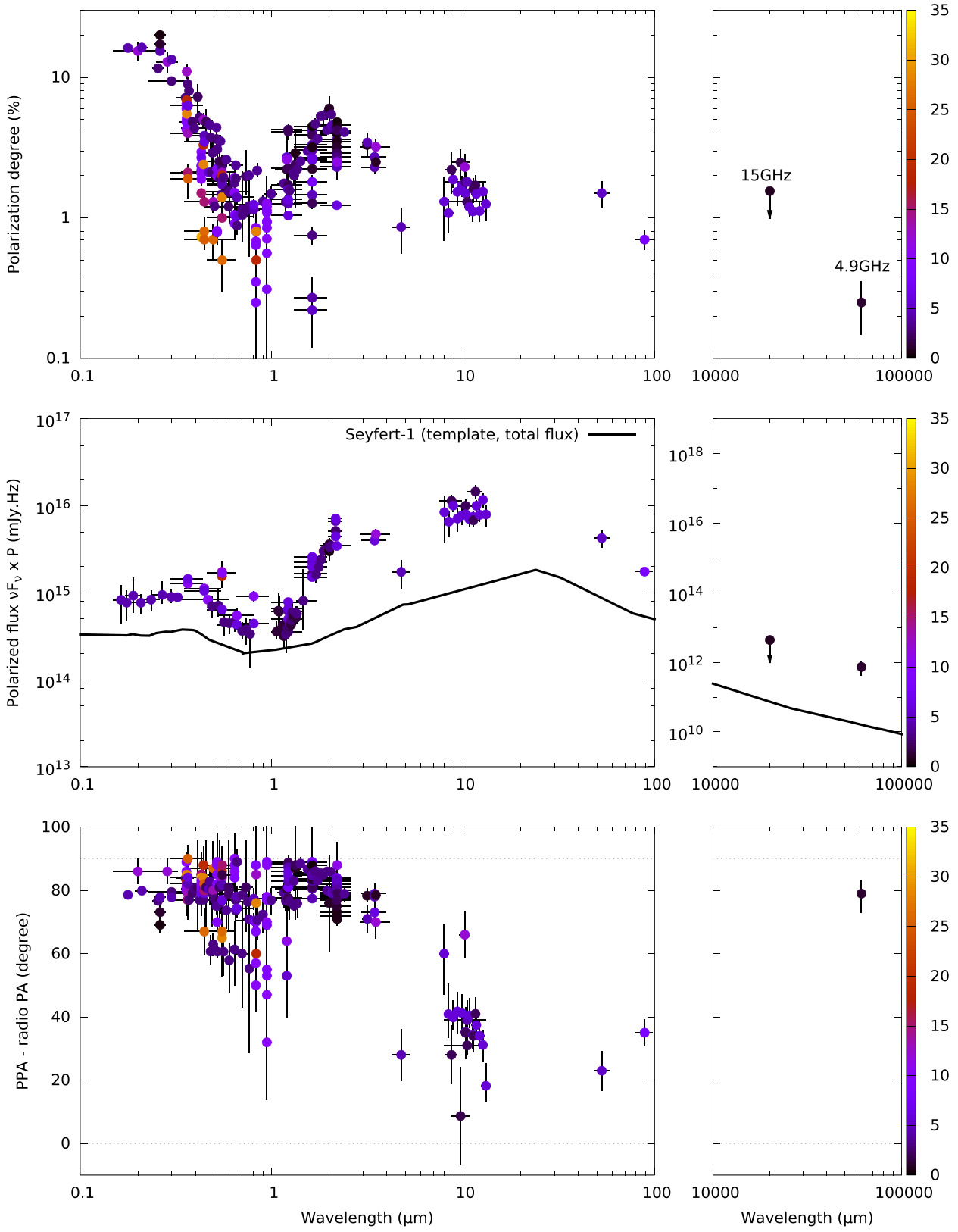

Figure 2. Broad-band 0.1–100 μm, 4.9, and 15 GHz continuum polarization of NGC 1068 measured from various instruments and apertures (colour-coded, in arcseconds). Instrumental and interstellar polarization have been accounted for, but contribution from the host galaxy is still present. See the text for details. Top: polarization degree, middle polarized flux (νF_ν, in mJy Hz, times P), bottom: PPA minus the parsec-scale radio PA. The Seyfert-1 total flux template presented in the polarized flux figure (middle) was shifted downwards for better visibility.

starlight contribution that almost cancel the observed polarization (Bolzonella et al. 2000). This polarization dip is also consistent with the transition waveband between the 'Big Blue Bump' and the 'infrared bump' detected in the SED of AGN. The Big Blue Bump is due to multicolour blackbody emission from the accretion disc and the infrared bump is attributed to thermal emission from dust (Sanders et al. 1989; Wilkes 2004). The inflection between the two bumps, related to dust sublimation at temperature 1500–2000 K, occurs at 1–2 μm, similarly to the onset of the infrared polarized peak. As it can be seen in Fig. 2, both the polarization degree and the polarized flux are strongly increasing in the near-infrared band. Interestingly, it appears that the polarized flux spectrum rises much more sharply in the near-infrared than the average type-1 SED that we have plotted. In this case, the orientation difference between NGC 1068 and the averaged SED of Prieto et al. (2010) certainly plays a role as polarization by polar scattering transitions in the infrared to polarization due to absorption/emission by aligned grains (this will be developed in the next paragraph). Polar scattering provides a similar face-on view to what we see in type-1 AGNs, but in the case of dichroic polarization, we are seeing the transmitted (or emitted) light from the edge on torus dust distribution.

At longer wavelengths, the host emission decreases and the infrared polarization shows a second maxima at wavelengths 2–3μm. The absence of variation seen in the PPA of light (which remains perpendicular to the axis of radio emission from the ultraviolet band to ∼3μm) indicates that most of the polarization is due to Thomson and Mie scattering in the polar region. However, at 4–5μm, the PPA switches from perpendicular to almost parallel. This effect was already highlighted and discussed by Bailey et al. (1988). The authors have shown that the angle rotation is not a consequence of the observed forbidden lines flux included in the passbands of the filters used, which would have the effect of pulling the PA towards the larger forbidden line value, but it is in fact a real feature of the continuum polarization. While the polarization in the ultraviolet, optical, and near-infrared bands is caused by polar scattering by electron and dust grains, the polarization at $\lambda \geq 4$ μm is most likely due to thermal emission from 100 pc dust grains aligned by large-scale magnetic fields (Efstathiou, McCall & Hough 1997; Lopez-Rodriguez et al. 2015). Since most of the dust is concentrated along the AGN equatorial plane, the polarization angle aligns with the radio axis and becomes parallel. The sharp decrease of polarized flux we observe at 4–5 μm confirms the variation of the cross-section of the scatterer. We are then able to trace the exact wavelength at which polar scattering becomes inefficient in NGC 1068.

In mid- and far-infrared bands, 10 μm polarization observations at sub-arcsecond resolution showed that the core of NGC 1068 becomes consistent with zero measured polarization; the main contributor to polarization is the extended emission that comes from the polar material / giant molecular clouds (GMC) interactions in the Northern ionization cones (Lopez-Rodriguez et al. 2016). Such discovery highlights the importance of correlating near- and mid-infrared data to draw conclusions. The polarized flux follows the dust emission by aligned grains and strongly increases between 10 and 20 μm. The polarized flux appears to reach a maximum in the uncharted 20–40 μm and far-infrared polarimetric measurements indicate that the polarized flux decreases in the 50–100 μm waveband.

Finally, in the radio band, two Very Large Array (VLA) measurements of the core polarization of NGC 1068 have been published. An upper limit was estimated at 15 GHz and the 4.9 GHz apparent polarization of the central AGN component is at the limit of accuracy of the measurement technique. Nevertheless, the polarized flux follows the expected trend of the type-1 total flux template with great consistency. The polarization degree is low, of the order of 0.25 per cent at 4.9 GHz and below 1.5 per cent at 15 GHz. Such low polarization degrees may be attributed to dilution by large quantities of thermal electrons as evidenced by the intense optical emission lines (Kraemer, Ruiz & Crenshaw 1998). The polarization angle could only be measured at 4.9 GHz and is essentially perpendicular to the source axis, similarly to the optical continuum polarization (e.g. Martin et al. 1983). We thus detect a second rotation of the PPA from the far-infrared to the radio domain. This rotation points toward a mechanism that is parallel to the polar magnetic fields. Accounting for the low polarization degree due to dilution by thermal electrons and the PPA that is perpendicular to the radio-axis, electron-scattered synchrotron emission appears to be the most plausible scenario (Gallimore, Baum & O'Dea 2004; Krips et al. 2006). This is in agreement with the work of Krips et al. (2006) who investigated several emission mechanisms to explain the millimetre-to-radio continuum emission in NGC 1068. Indeed, the authors concluded that 'the core fluxes indicate a turnover of the inverted cm- into a steep mm-spectrum at roughly 50 GHz, which is most likely caused by electron-scattered synchrotron emission'.

In conclusion, it is truly remarkable to observe that the whole polarized SED of NGC 1068 is following the averaged total flux type-1 SED extracted from Prieto et al. (2010), proving that a type-1 core genuinely resides inside NGC 1068. We also note that the different emission and reprocessing mechanisms have a deep impact on to the PPA, allowing us to probe the physics inside the core of obscured AGN.

2.3 Impact of aperture on to the observed polarization

It is well known that the measured AGN polarization depends on the aperture used (see e.g. Bailey et al. 1988). The better we isolate the compact nucleus from the host starlight and starburst activity, the higher the ultraviolet, optical, and near-infrared polarization degree.[5] This effect is clearly visible in Fig. 2, where the color-code highlights the fact that polarimetric measurements with large apertures are always smaller than polarimetric observations at the same wavelength with a smaller observational aperture. Yet, since our catalogue compiles all polarimetric data recorded for NGC 1068, we can investigate the impact of aperture on to the resulting polarization with better accuracy. We isolate two regions from Fig. 2 where the polarization degree is found to vary over several percentage points at a given wavelength: around 4450 Å (*B* band) and around 2.2 μm (*K* band). The polarization dependency on the aperture is shown in Fig. 3 (top: polarization degree, bottom: polarization angle). The aperture varies from 2.8 to 30.6 arcsec in the blue band and from 0.2 to 11 arcsec in the infrared, which corresponds to 205–2250 and 14–810 pc, respectively. We see that the observed polarization degree indeed increases gradually as we get closer to the active nucleus. Dilution by the host is relatively important for large apertures and the polarization degree exponentially increases when the observer reaches apertures lower than 15 arcsec. We fitted the data point using exponential function that are summarized in Table 2. All fits have a coefficient of determination R^2, which is the proportion

[5]Thanks to high angular-resolution polarimetric observations, Packham et al. (2007) and Lopez-Rodriguez et al. (2016) have shown that the 10 μm polarization decreases with decreasing aperture. This is due to the complex combination of (i) the extended emission from the wind-GMC interaction in the Northern ionization cones, (ii) the absorption polarization in the Southern

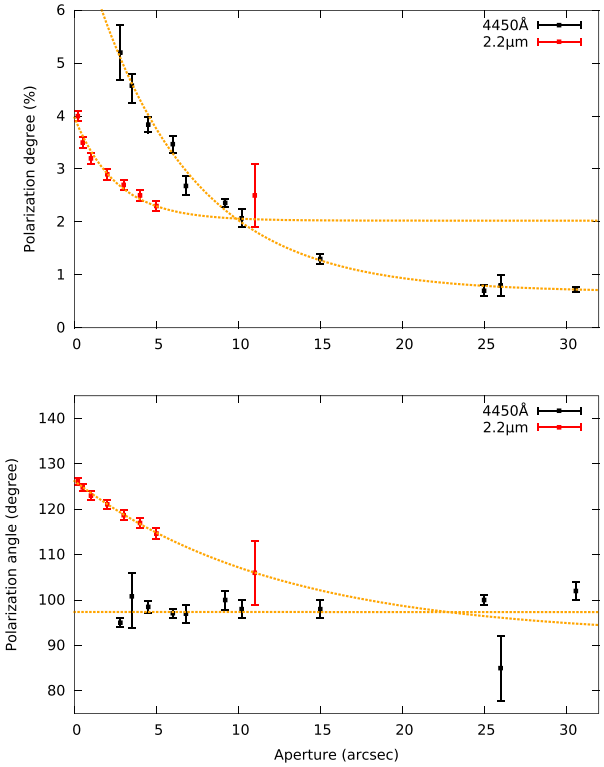

Figure 3. Aperture effect on the measured continuum polarization of NGC 1068 around 4450 Å (in black) and around 2.2 μm (in red). The first panel shows the variations of the polarization degree, and the second panel is for the PPA. Fits to the data are shown in orange dashed lines.

Table 2. Fits to variation of polarization degree P and PPA Ψ as a function of aperture Ap from Fig. 3. The coefficient of determination R^2 is indicated in the second column.

$P_{4450} = 0.68 + 6.99^{*}\exp(-0.16^{*}\mathrm{Ap})$	$R^2 > 0.99$
$P_{2.2\,\mu m} = 2.02{+}1.95^{*}\exp(-0.39^{*}\mathrm{Ap})$	$R^2 > 0.97$
$\Psi_{4450\,Å} = -0.49.10^{-4}{*}\mathrm{Ap} + 97.37$	$R^2 < 0.01$
$\Psi_{2.2\,\mu m} = 91.90 + 34.34^{*}\exp(-0.08^{*}\mathrm{Ap})$	$R^2 > 0.99$

of the variance in the dependent variable that is predictable from the independent variable, superior to 0.97. However, there is no evidence for a variation in the PPA at 4450 Å as aperture increases. Overall, we find a clear exponential dependence of the polarization properties with respect to the observational aperture. Our fits can then help to predict the expected polarization degree and angle at a given aperture for a given waveband. Additional polarimetric observations are needed in a large variety of wavebands to generalize our equations.

The observed polarization plateaus and the rotation of the PPA indicate the presence of large-scale polarization that can only be attributed to the host itself. Scattering of starlight by dust, molecules, and electrons in the galactic medium is known to produce a low amount of optical polarization that depends on the orientation of the host plane (Scarrott et al. 1991; Simmons & Audit 2000). For an edge-on galaxy, the expected large-scale polarization lies between 0.8 and 1.8 per cent (Simmons & Audit 2000). The former value well corresponds to the plateau reached by the optical polarization curve in Fig. 2 (top). This polarization degree is in agreement with the optical linear polarization maps of NGC 1068 obtained by Scarrott et al. (1991), who have shown that the polarization data from $r < 10$ arcsec traces the large-scale structure of the host. The spiral structure of the host, forming a roughly circularly symmetric pattern, almost certainly accounts for some of the decrease in polarization as the aperture size increases. At longer wavelength, near-infrared polarimetry of a normal spiral galaxy allowed Clemens, Pavel & Cashman (2013) to show that the polarization fraction of late-type galaxies can reach up to 3 per cent, which also corresponds to the plateau of 2.2 μm polarization we found. In conclusion, the diversity of apertures used to achieve polarimetric observations of NGC 1068 allowed us to confirm the amount of optical and near-infrared polarization from its host.

Additionally, according to Schmitt & Kinney (1996) and Murayama & Taniguchi (1997) the optical size of the extended narrow line region in NGC 1068 is about 900 pc (12.25 arcsec), which roughly corresponds to the inflexion point of the optical polarization fit as a function of aperture in Fig. 3. Since most of the low-aperture optical continuum polarization we observe from NGC 1068 is due to scattering of disc photons inside the polar outflows, and since we have demonstrated that large aperture polarization is dominated by the host, we can safely confirm that the extension of the narrow line region probably stops before 1030 pc. This value is at a safe distance from the abrupt fall in the surface brightness profile of NGC 1068 observed by Sánchez-Portal et al. (2004) and that is situated around 2.2 kpc from the centre of the galaxy.

Consequently, despite the fact that the compiled continuum polarization spectrum of NGC 1068 presented in Fig. 2 suffers from the various apertures used, we know from Table 1 that only a few observations were done with apertures larger than the estimated extension of the scattering outflows. This indicates that most of the data have indeed measured the polarization originating mainly from the first hundreds of parsecs surrounding the AGN core and that the features we see in Fig. 2 are not artefacts. Even if all the different apertures do play a role, they only contribute to a lesser extent to the characteristic wavelength-dependent polarization profile.

2.4 Reconstructing the spectral energy distribution

Correcting the continuum polarization from diluting light is a major complication. While it is important to estimate the instrumental polarization and the contamination by interstellar polarization, it is crucial to remove the dilution by starlight in order to study the wavelength dependence of polarization (Miller & Antonucci 1983). To do so, the aforementioned authors carried out observations of M32, a morphologically classified compact elliptical galaxy, in order to remove any unpolarized starlight that is dominating the continuum polarization of NGC 1068 longwards of 4000 Å. By minimizing the stellar absorption features in the residuals of the M32/NGC 1068 flux ratio spectra, Miller & Antonucci (1983) derived the following starlight fractions in the observed AGN continuum flux: 0.42 at 3600 Å, 0.63 at 4200 Å, 0.78 at 4600 Å, and 0.82 at 5075 Å (with 5 per cent uncertainty). They corrected their linear polarization spectrum and found a wavelength-independent polarization of 16 ± 2 per cent in the 3500–5200 Å waveband. However, to achieve so, high-resolution (<10 Å) spectropolarimetry is necessary. Most of the published polarimetric measurements of NGC 1068 were achieved in narrow-band filters, which prevent us to use this method.

cone, and (iii) the unpolarized core from self-absorbed dichroic emission from the torus.

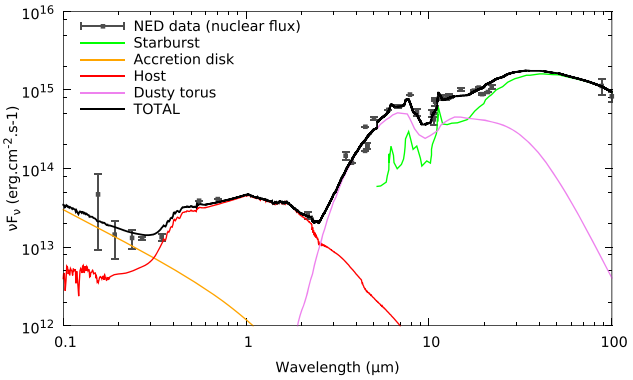

Figure 4. Observed nuclear fluxes of NGC 1068 (grey squares) extracted from the NED. See the text for details about the emissive components used to reproduce the broad-band SED.

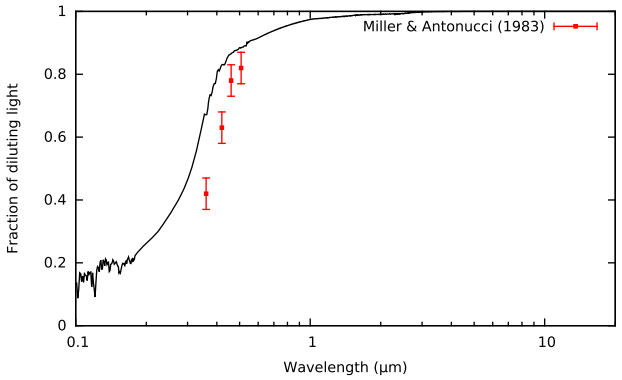

Figure 5. Derived fraction of diluting light (starlight plus dust emission components) in the observed continuum flux of NGC 1068. The previous estimation made by Miller & Antonucci (1983) using a circular aperture of 2.8 arcsec is shown in red.

We thus opted for a similar procedure that rather focuses on the continuum flux of NGC 1068. We extracted from the NASA/IPAC Extragalactic Database (NED) all the nuclear observations of NGC 1068 and plotted them in Fig. 4. We focused on nuclear fluxes in order to better estimate the fraction of starlight in the observed continuum flux of NGC 1068. We reconstructed the 0.1–100 μm SED of NGC 1068 using usual AGN components: the scattered light of a thermally emitting multicolour accretion disc, a component reproducing the infrared re-emission of the circumnuclear AGN torus, a template for the host galaxy, and a template for the starburst light contribution.

(i) To construct the accretion disc SED, we used the standard thin disc model (Shakura & Sunyaev 1973). The accretion disc spans from 1 to 1000 gravitational radii and surrounds a 8.10^6 solar mass black hole (Lodato & Bertin 2003) accreting at 0.4 times the Eddington rate (Kumar 1999). The inclination of the disc was fixed to 85° according to the numerical reconstruction of NGC 1068 achieved by Fischer et al. (2013, 2014). The question about the true inclination of the system remains opened (Marin, Goosmann & Petrucci 2016), but we checked that varying those parameters only marginally influence the power-law shape of the scattered light of the disc SED observed in the ultraviolet–optical band. The variations are within the expected range of values (power-law index $\sim$ 1/3 due to the superposition of blackbodies).

(ii) Dust re-emission by the obscuring equatorial torus is simulated using the model presented by Fritz, Franceschini & Hatziminaoglou (2006) to fit the infrared SED of NGC 1068. The toroidal model has an aperture angle of 160°, an optical depth of 8 at 9.7 μm, and is characterized by multiple grain temperatures set by thermal equilibrium equations. The torus extends up to 16.4 pc, has an outer-to-inner radii ratio of 20 and its dust density distribution varies both in the radial and in the altitude coordinates. We note that Fritz et al. (2006) used a homogeneous distribution of dust to describe the torus; in reality Atacama Large Millimeter/sub-millimeter Array (ALMA) has shown that the outer edge of the torus is likely to be clumpy (Gallimore et al. 2016; García-Burillo et al. 2016). Its outer radius is of the order of 10 pc but most of the obscuring material of the torus is concentrated around 5 pc, according to the clumpy torus models (García-Burillo et al. 2016). This results in a model that may overestimate the far-infrared/millimetre emission that is, in any case, extended.

(iii) A template for the host galaxy has been extracted from Bruzual & Charlot (1993) and was extended towards the ultraviolet and infrared bands by Bolzonella et al. (2000). It corresponds to an archetypal Sbc barred spiral galaxy, which is consistent with the classification of the host of NGC 1068 (Balick & Heckman 1985). The initial mass function by Miller & Scalo (1979) was used with an upper mass limit for star formation of 125 $M_\odot$. The data base used to compute this SED includes only solar metallicity, but it appears to have a minimum impact on to the resulting template (Bolzonella et al. 2000).

(iv) Finally, starburst activities are present in the central kiloparsec of NGC 1068 (Lester et al. 1987; Romeo & Fathi 2016), imprinting the 5–100 μm infrared band with strong features (Thronson et al. 1989; Le Floc'h et al. 2001). Following Fritz et al. (2006), we included a starburst component needed to reproduce the intensity of the polycyclic aromatic hydrocarbon features between 6 and 15 μm, as well as the depth of the silicate feature at 9.7 μm, and the width, intensity and peak wavelength of the infrared bump. To do so, we include the contribution of the infrared spectrum of the starburst galaxy NGC 7714 that correctly reproduces the colder component of dust emission (Fritz et al. 2006).

Our final SED is presented in black in Fig. 4 and it satisfactorily reproduces observations (in grey). This SED has been chosen to minimize the differences between the model and the observed fluxes but we remark slight degeneracies due to the data errors bars, particularly in the ultraviolet and blue bands. Nevertheless, the shape of the near and mid-infrared spectrum is very well reproduced using a generic template for the host rather than using a specific galaxy observation such as M32. The transition between disc emission and torus emission happens at the expected wavelength and the host galaxy indeeds dominates the continuum flux of NGC 1068 longwards of 3000 Å.

2.5 Polarization correction

The overall agreement between the observed data points and our SED model allows us to derive the fraction of starlight plus dust emission components (dust-reprocessed accretion disc emission and starburst emission) in the observed continuum flux of NGC 1068. The flux ratio is shown in Fig. 5, together with the ratios derived by (Miller & Antonucci 1983) using the M32 template. Although the ratios are not the same (this being due to the two different approaches: spectropolarimetric fitting versus SED fitting, the former being unfeasible in this paper), the shape of the wavelength-dependent ratios is distinctively similar. In our model, the host

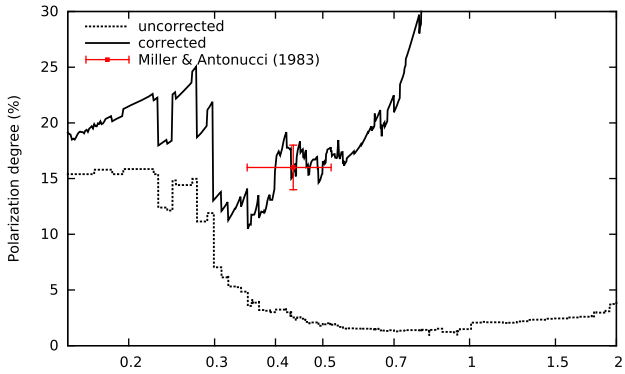

Figure 6. Corrected average continuum polarization of NGC 1068 using the fraction of diluting light (starlight plus dust emission components) in the observed continuum flux presented in Fig. 5. The previous estimation made by Miller & Antonucci (1983) is shown in red.

galaxy starlight starts at bluer wavelengths, hence the shift by almost 1000 Å. We tried to reproduce the exact same flux ratios estimated by (Miller & Antonucci 1983) by changing the normalization of our SED components but the observed data points were no longer matched in the optical band. We stress that this is a logical outcome: first there is a difference in the apertures being used; second the two host galaxy SED used in Miller & Antonucci (1983) and in our paper are not the same. In particular, the choice of M32 may have had consequences on the spectropolarimetric analysis. M32 is an elliptical satellite galaxy of the M31 sub-group, together with NGC 205. A giant stream in the outer halo of M31, pointed in the direction of M32, was observed by Ibata et al. (2001), leading to potential tidal interaction between the galaxies (Choi, Guhathakurta & Johnston 2002). But despite the morphological and chemical differences between the two templates, the most important investigation is to test whether our SED and the fraction of starlight plus dust emission components in the observed continuum flux of NGC 1068 can reproduce the expected polarization thresholds quoted by Miller & Antonucci (1983) and Antonucci & Miller (1985).

In Fig. 6, we present the averaged combined polarization spectrum of NGC 1068 taken from Fig. 2 (dashed line), together with the linear continuum polarization corrected for (1) the host starlight dilution and (2) the dust emission components, both the torus (i.e. reprocessed accretion disc emission) and the starburst dust emission, using the derived fraction of diluting light in the observed continuum flux of NGC 1068 (Fig. 5). We added the measure by Miller & Antonucci (1983) in red and we cut the spectrum at 2 μm since dust re-emission is dominating at longer wavelengths. Our correction to the averaged compiled polarization spectrum of NGC 1068 reproduces the measurement by Miller & Antonucci (1983) in the optical band. Our data indicate a median polarization of 17 ± 3 per cent in the 3000–7000 Å band while Miller & Antonucci (1983) estimated a continuum polarization of 16 ± 2 per cent in the 3500–5200 Å waveband. Our method is subject to higher polarization fluctuations due to the large range of observational apertures used but gives reliable estimation of the true scattered polarization of Seyfert-2 AGN. The sharp features at ∼0.22 and ∼0.3 μm are directly caused by the lack of polarimetric measurements in several consecutive bins (as it can be seen in the uncorrected spectrum in dashed line that sharply decreases at those wavelengths). It also appears that the continuum polarization increases in the ultraviolet due to dust scattering at distances larger than 1 arcsec from the AGN core (Antonucci, Hurt & Miller 1994). This is in complete agreement with the discovery of Hönig et al. (2013) and Asmus, Hönig & Gandhi (2016), who have shown that optically thin dust in the polar outflows is responsible for much for the observed mid-infrared flux. The ultraviolet wavelength-dependent polarization signature we observe in Fig. 6 (for apertures greater than 1 arcsec) is naturally explained by scattering of light by dust particles along the polar direction. In the near-infrared band, the asymptotic behavior of the dilution-corrected polarization spectrum is a consequence of the fact that the accretion disc continuum decreases relative to the stellar continuum, as wavelength increases. Nevertheless, we demonstrated that it is possible to build a reliable combined spectrum of the optical linear continuum polarization of AGN from published data despite the diluting action of the host galaxy and dust emission components.

2.6 Temporal evolution of the continuum polarization

The last aspect of our study is to test whether the polarization of NGC 1068 has significantly evolved in time. We know that the observed polarization does not linearly depend on the amount of photons produced by the central engine. The chaotic light curve of AGN does not change the polarization state unless the powerful radiation field wipes out a fraction of the material in the vicinity of the black hole (see e.g. Jackson & Browne 1990; Lawrence 1991; Hill, Goodrich & Depoy 1996). Even in this case, the amount of material removed by the radiation field must be significant to alter the polarimetric signature of the AGN in a detectable fashion (Marin et al. 2016). The dynamical time-scales for changing the geometric arrangement of matter or magnetic fields at (sub-)parsec-scales around a 10^8 solar masses black hole is of the order of 5–100 yr (Hopkins et al. 2012). Only long-term monitoring of the polarization of a given AGN can probe such changes.

We present in Fig. 7 the time evolution of the continuum polarization of NGC 1068 in several wavebands from the optical to the infrared domain. A similar aperture, indicated in each plot, was chosen when compiling the published data in order not to include systematic effects. There can still be (for the smallest apertures) a small impact of the seeing but this is likely mitigated by the use of a range of apertures rather than a single aperture. As it can be seen, the polarization degree does not change by more than a fraction of a percentage point over several decades. If the error bars of the first and last polarimetric points in the 3800–4880 Å and 1.8–2.6 μm figures are real, then there is a tentative statistically significant increase of polarization with time but the polarization angle (not shown) remains constant. This could coincide with the variability of the near-infrared nuclear flux of NGC 1068 observed between 1976 and 1994 by Glass (1997). From his study, it was not clear whether this event has been the response of an extended dusty region to a single outburst in the central engine or the result of a continuous change in its ultraviolet output, but it was shown in Marin et al. (2016) and Marin (2017) that parsec-scale morphological changes in the geometry of the AGN would have varied the observed polarization degree by several percentage points and may be accompanied by a rotation of the PPA. It is then safe to say that the global morphologic and magnetic geometry of NGC 1068 probably did not change since 1975. The 1965–1975 period could not be investigated due to the large apertures used at that time, but it is unlikely that a strong change happened in less than a decade. Overall, we have proven that NGC 1068 remained remarkably constant in terms of polarimetry over the past 50 yr.

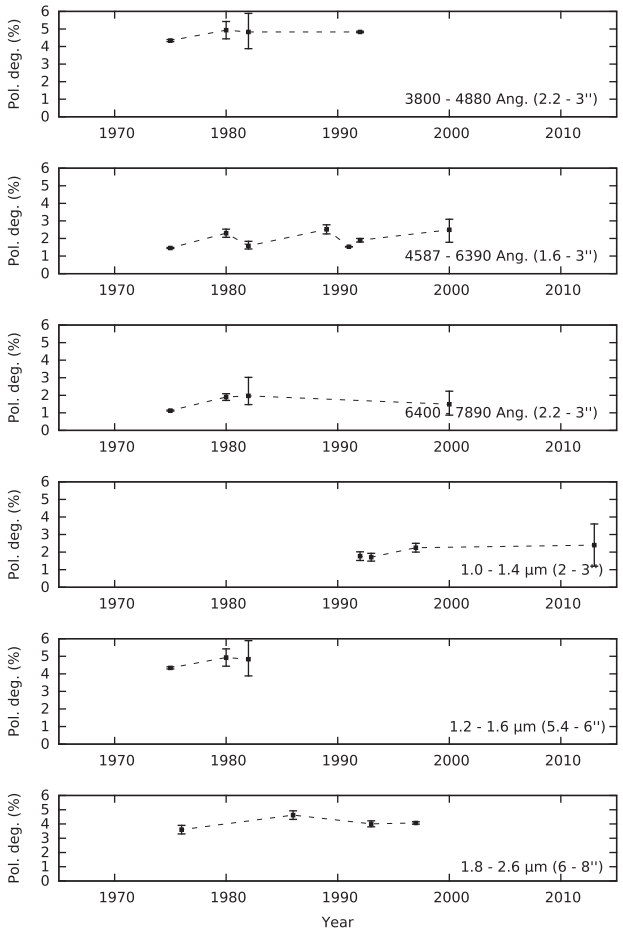

Figure 7. Time evolution of the polarization degree of NGC 1068 in several wavebands at a fixed aperture.

3 MULTIWAVELENGTH POLARIMETRY OF AGN: WHAT IS MISSING?

Reconstructing the polarization spectrum of an AGN is a difficult task since polarimetric data are easily contaminated by starlight, Galactic dust, starburst light, and interstellar polarization. However, we have shown that the polarimetric spectrum of NGC 1068, despite the diversity of instruments and apertures, has distinctive wavelength-dependent signatures that can be related to the AGN and host galaxy physics. Impact of the Big Blue bump and infrared bump, electron, Mie and dichroic scattering, synchrotron emission and radio dilution by thermal electron is naturally highlighted in polarization. This is the reason why polarimetry remains one of the best methods to explore the geometry and physics of unresolvable/obscured cosmic sources. Nevertheless, an important fraction of the polarized spectrum of NGC 1068 remains unexplored.

The X-ray band is a territory where no polarimetric information has ever been recorded in the case of AGN. X-ray polarization is expected to arise from electron, dust and gas scattering, as well as magnetic processes (McNamara, Kuncic & Wu 2009). Compton and inverse-Compton scattering are the dominant processes, similarly to Thomson and Mie scattering in the optical band, and the expected X-ray polarization can be evaluated (at first order) by looking at the visual polarization (Marin et al. 2016). In addition, since the X-ray continuum is produced close to the central supermassive black hole, special and general relativistic effects are expected to impact the observed polarization properties of light (e.g. Connors & Stark 1977; Pineault 1977; Connors, Stark & Piran 1980). Due to strong gravity effects, the polarization direction rotates along the photon null geodesics as the polarization vector is parallelly transported, resulting in specific polarimetric features. By observing the X-ray polarization of compact objects, it becomes possible to characterize the mass of the black hole, its spin, the composition of the accretion disc, and the geometry of the system (Dovčiak et al. 2004; Schnittman & Krolik 2009, 2010; Marin & Weisskopf 2017; Marin et al. 2018).

The far-ultraviolet band offers unique insight into the physics of AGN that is still little known, in particular by probing ultraviolet-emitting and absorbing material arising from accretion discs, synchrotron emission in jet-dominated AGN, and large-scale outflows. Some key signatures of accretion discs can be revealed only in polarized light, and with higher contrast at ultraviolet than at longer wavelengths (Kishimoto et al. 2008). Specifically, ultraviolet polarimetry can provide geometrical, chemical, and thermodynamical measurements of accretion discs at unprecedented resolutions. By probing the ubiquitous magnetic fields, which are expected to align non-spherical small dust grains on the scales of the accretion disc to the extended torus, a future ultraviolet polarimeter such as POLLUX on-board of LUVOIR (Bolcar et al. ; Bouret et al. 2018) will be able to reveal the mechanisms structuring the multiscale AGN medium.

Far-infrared polarimetry remains an almost uncharted waveband despite the fact that observations do not suffer from seeing problem, allowing to deeply probe high extinction areas. Polarimetric measurements of ultra-luminous galaxies would allow one to address a variety of issues such as the nature of the emission that could be either non-thermal or originating from dust. By detecting solid-state spectral features, far-infrared polarimetry should be able to discriminate between thermal and non-thermal emission in AGN, such as starburst galaxies (Bressan, Silva & Granato 2002; Andreani et al. 2003). The large-scale polarimetric signature most likely originates from extended magnetic fields that align dust grains. The associated dichroic absorption and emission mechanisms provide information on the geometry of the magnetic fields, which is essential to better understand accretion processes, disc formation, and mass outflows from stars to AGN (Hough & Aitken 2003).

Polarimetric imaging in the (sub)millimetre offers the possibility of identifying magnetic field configurations at unprecedented scales. Using ALMA, we can resolve the torus outer regions and study the polarized dust emission by dichroic emission and absorption by aligned grains. In particular, Aitken et al. (2002) have shown that sub-millimetre polarization can lead to strong constraints on the field configuration for a variety of torus models. Circular polarization, which is easily acquired at those wavelengths, could also enlighten us on the jet structure of AGN (Sazonov 1969). The POLAMI programme (Agudo et al. 2018a,b; Thum et al. 2018) is using the fact that Faraday conversion can convert linear polarization to circular polarization to probe the magnetized plasma of jet in a large sample of radio-loud AGN.

Finally AGN radio polarization measurements are possible as synchrotron emission is naturally highly polarized when magnetic field lines are ordered (Westfold 1959). However, in the case of radio-quiet AGN polarization, the GHz and MHz bands remain largely unexplored as Seyfert galaxies are generally reported to be unpolarized in the radio band, even in the optically thin regions (Antonucci 1993). Yet those measurements have been achieved almost four decades ago and NGC 1068 appears to be (weakly) polarized at 4.9 GHz. New observations with modern radio telescopes are

necessary to explore with better sensitivity the emission and reprocessing mechanisms in the radio band. In particular, the turnover frequency between dust polarized emission and synchrotron polarization could be detected by discovering the wavelength at which the PPA rotates.

4 SUMMARY AND CONCLUSIONS

We have gathered all the published polarimetric information on NGC 1068, the most observed Seyfert galaxy in terms of polarimetry. We compiled the broad-band 0.1–100μm, 4.9, and 15 GHz continuum polarization of this archetypal type-2 AGN using data from more than 50 yr of observations, a premiere in the field. By doing so, we were able to detect all the expected transition regions in the polarized SED of NGC 1068: the Big Blue Bump (0.1–0.7 μm), the peak of starlight contribution (∼1 μm), the infrared bump (1–4 μm), and the transition between electron scattering and polarized dust reemission (4–5 μm). Additional radio measurements also point towards another polarization mechanism linked with synchrotron emission, scattering and dilution by thermal electrons, highlighted by a rotation of the PPA between the far-infrared and the radio bands. Despite the large variety of apertures and instruments used, the wavelength-dependent behaviour of the polarization clearly revealed the wavebands where processes are switching. This work allowed us to reconstruct the broad-band polarized SED of NGC 1068, which strongly resembles to a typical type-1 SED seen in total flux. We analyzed the aperture effect on the measured continuum polarization of NGC 1068 and found a large-scale polarization component that can only be attributed to the host itself. This constant value for high apertures corresponds to the measured polarization degree of regular spiral galaxies, confirming previous observational results (Scarrott et al. 1991; Simmons & Audit 2000). For apertures lower than 15 arcsec, the degree of polarization exponentially increases since the aperture gets smaller than the scattering region size, highlighting the presence of the narrow line region.

In order to carefully remove the contribution of starlight to the continuum polarization of our compiled spectrum, we reconstructed the global SED of NGC 1068 using nuclear fluxes from NED and a set of emissive components. By doing so, we were able to derive the fraction of starlight in the observed continuum flux of NGC 1068. We corrected our 0.15–2 μm continuum polarization spectrum and found a wavelength-independent polarization level in the optical band, such as expected from theory and past studies. We also highlighted the impact of dust scattering in the ultraviolet and near-infrared bands for larger apertures (electron scattering is dominating from the ultraviolet to the near-infrared at arc-second scale apertures). Finally, we checked whether the observed polarimetric signal of NGC 1068 varied through time. We demonstrated that this particular AGN did not undergo a major morphological or magnetic change over the past decades since its polarimetric signal remained constant (at similar apertures and in the same waveband).

In conclusion, we have created the very first broad-band compiled polarization spectrum of an AGN exploiting more than 50 yr of data. The results are in strong agreements with the Unified Scheme of AGN despite the scarcity of data at several wavebands. Large class (30 m) telescopes equipped with polarimeters are needed to pursue the study at deeper levels, both in spectroscopic and imaging modes. Despite being restricted to 0.1–100 μm, plus two points in the centimetre band, the work achieved in this paper can now be compared to the results of Monte Carlo radiative transfer simulations in order to test different geometries of the reprocessing and emitting media (e.g. Goosmann & Gaskell 2007; Marin et al. 2012; Marin, Goosmann & Gaskell 2015; Rojas Lobos et al. 2017; Grosset et al. 2017; Marin 2018). This is an important step as, so far, any model-to-data comparison was only achieved in narrow bands. We also highlight the fact that our study could be expanded by many orders of magnitude by looking at the radio, millimetre, far-infrared, far-ultraviolet, and X-ray polarization of AGN using ALMA, HAWK+, or the forthcoming satellites IXPE (Weisskopf et al.), eXTP (Zhang et al.), and LUVOIR (Bolcar et al. ; Bouret et al. 2018).

ACKNOWLEDGEMENTS

This paper is a tribute to all the observers who dedicated their career to better understand AGN using polarimetry. I would like to thank (in alphabetical order) Beatriz Agís González, Robert Antonucci, Lucas Grosset, Damien Hutsemékers, Enrique Lopez Rodriguez, Makoto Kishimoto, Chris Packham, Dominique Sluse, Yelena Stein, and Bernd Vollmer for their numerous comments and suggestions that greatly improved this paper. Georges Roudnitski, from the Astronomicheskii Tsirkulyar journal, was of a great help to retrieve and translate old Russian papers. I also acknowledge the anonymous referee who helped to clarify and improve this paper. Finally, the author would like to thank the Centre national d'études spatiales (CNES) who funded this project through to the post-doctoral grant 'Probing the geometry and physics of active galactic nuclei with ultraviolet and X-ray polarized radiative transfer'.

REFERENCES

Agudo I., Thum C., Ramakrishnan V., Molina S. N., Casadio C., Gómez J. L., 2018a, MNRAS, 473, 1850
Agudo I. et al., 2018b, MNRAS, 474, 1427
Aitken D. K., Briggs G., Bailey J. A., Roche P. F., Hough J. H., 1984, Nature, 310, 660
Aitken D. K., Efstathiou A., McCall A., Hough J. H., 2002, MNRAS, 329, 647
Alexander D. M., Young S., Hough J. H., 1999, MNRAS, 304, L1
Andreani P., Cristiani S., Grazian A., La Franca F., Goldschmidt P., 2003, AJ, 125, 444
Angel J. R. P., Stockman H. S., Woolf N. J., Beaver E. A., Martin P. G., 1976, ApJ, 206, L5
Antonucci R., 1993, ARA&A, 31, 473
Antonucci R., Hurt T., Miller J., 1994, ApJ, 430, 210
Antonucci R. R. J., 1982, Nature, 299, 605
Antonucci R. R. J., 1984, ApJ, 278, 499
Antonucci R. R. J., Miller J. S., 1985, ApJ, 297, 621
Asmus D., Hönig S. F., Gandhi P., 2016, ApJ, 822, 109
Bailey J., Axon D. J., Hough J. H., Ward M. J., McLean I., Heathcote S. R., 1988, MNRAS, 234, 899
Balick B., Heckman T., 1985, AJ, 90, 197
Barthel P. D., 1989, ApJ, 336, 606
Bauer F. E. et al., 2015, ApJ, 812, 116
Blaes O., Agol E., 1996, ApJ, 469, L41
Blaes O., Agol E., 1997, in Wickramasinghe, D. T. , Bicknell, G. V., Ferrario, L., eds, ASP Conf. Ser. Vol. 202, IAU Colloq. 163: Accretion Phenomena and Related Outflows. Astron. Soc. Pac., San Francisco, p. 610
Bolcar M. R., Feinberg L., France K., Rauscher B. J., Redding D., Schiminovich D., 2016,Proc. SPIE Conf. Ser. Vol. 9905, SPIE Astronomical Telescopes and Instrumentation, SPIE, Bellingham, p. 99040J
Bolzonella M., Miralles J.-M., Pelló R., 2000, A&A, 363, 476
Bouret J.-C. et al., 2018, American Astronomical Society Meeting Abstracts, 231, 419.01
Bressan A., Silva L., Granato G. L., 2002, A&A, 392, 377
Bruzual A. G., Charlot S., 1993, ApJ, 405, 538

Capetti A., Axon D. J., Macchetto F., Sparks W. B., Boksenberg A., 1995a, ApJ, 446, 155
Capetti A., Macchetto F., Axon D. J., Sparks W. B., Boksenberg A., 1995b, ApJ, 452, L87
Choi P. I., Guhathakurta P., Johnston K. V., 2002, AJ, 124, 310
Clemens D. P., Pavel M. D., Cashman L. R., 2013, AJ, 145, 74
Code A. D., et al., 1993, ApJ, 403, L63
Connors P. A., Stark R. F., 1977, Nature, 269, 128
Connors P. A., Stark R. F., Piran T., 1980, ApJ, 235, 224
Dibai E. A., Shakhovskoi N. M., 1966, Astronomicheskij Tsirkulyar, Eurasian Astronomical Society and Sternberg Astronomical Institute, Moscow, Russia, p. 375
Dombrovskii V. A., Gagen-Torn V. A., 1968, Astrophysics, 4, 163
Donahue M. et al., 2015, ApJ, 805, 177
Dovčiak M., Karas V., Matt G., 2004, MNRAS, 355, 1005
Dovčiak M., Muleri F., Goosmann R. W., Karas V., Matt G., 2011, ApJ, 731, 75
Dyck H. M., Jones T. L., 1976, BAAS, 8, 568
Efstathiou A., McCall A., Hough J. H., 1997, MNRAS, 285, 102
Elvius A., 1978, A&A, 65, 233
Elvius A., Hall J. S., 1965, AJ, 70, 138
Fischer T. C., Crenshaw D. M., Kraemer S. B., Schmitt H. R., 2013, ApJS, 209, 1
Fischer T. C., Crenshaw D. M., Kraemer S. B., Schmitt H. R., Turner T. J., 2014, ApJ, 785, 25
Fritz J., Franceschini A., Hatziminaoglou E., 2006, MNRAS, 366, 767
Gallimore J. F., Baum S. A., O'Dea C. P., 2004, ApJ, 613, 794
Gallimore J. F. et al., 2016, ApJ, 829, L7
García-Burillo S. et al., 2016, ApJ, 823, L12
Gehrels T., 1972, ApJ, 173, L23
Glass I. S., 1997, Ap&SS, 248, 191
Goosmann R. W., Gaskell C. M., 2007, A&A, 465, 129
Gratadour D., Rouan D., Grosset L., Boccaletti A., Clénet Y., 2015, A&A, 581, L8
Grosset L., Rouan D., Gratadour D., Pelat D., Orkisz J., Marin F., Goosmann R., 2018, A&A, 612, A69
Hill G. J., Goodrich R. W., Depoy D. L., 1996, ApJ, 462, 163
Hopkins P. F., Hayward C. C., Narayanan D., Hernquist L., 2012, MNRAS, 420, 320
Hough J. H., Aitken D. K., 2003, J. Quant. Spectrosc. Radiat. Transfer, 79, 733
Hönig S. F., Prieto M. A., Beckert T., 2008, A&A, 485, 33
Hönig S. F. et al., 2013, ApJ, 771, 87
Ibata R., Irwin M., Lewis G., Ferguson A. M. N., Tanvir N., 2001, Nature, 412, 49
Imanishi M., Nakanishi K., Izumi T., Wada K., 2018, ApJ, 853, L25
Jackson N., Browne I. W. A., 1990, Nature, 343, 43
Khachikian E. Y., Weedman D. W., 1974, ApJ, 192, 581
Kishimoto M., 1999, ApJ, 518, 676
Kishimoto M. et al., 2008, Nature, 454, 492
Knacke R. F., Capps R. W., 1974, ApJ, 192, L19
Kraemer S. B., Ruiz J. R., Crenshaw D. M., 1998, ApJ, 508, 232
Krips M. et al., 2006, A&A, 446, 113
Kruszewski A., 1971, Acta Astron., 21, 311
Kruszewski A. K., 1968, AJ, 73, 852
Kumar P., 1999, ApJ, 519, 599
Landstreet J. D., Angel J. R. P., 1972, ApJ, 174, L127
Lawrence A., 1991, MNRAS, 252, 586
Lebofsky M. J., Kemp J. C., Rieke G. H., 1978, ApJ, 222, 95
Le Floc'h E., Mirabel I. F., Laurent O. et al., 2001, A&A, 367, 487
Lester D. F., Joy M., Harvey P. M., Ellis H. B., Jr, Parmar P. S., 1987, ApJ, 321, 755
Lodato G., Bertin G., 2003, A&A, 398, 517
Lopez-Rodriguez E. et al., 2015, MNRAS, 452, 1902
Lopez-Rodriguez E. et al., 2016, MNRAS, 458, 3851
Low F. J., Rieke G. H., 1971, Nature, 233, 256
Lumsden S. L., Moore T. J. T., Smith C., Fujiyoshi T., Bland-Hawthorn J., Ward M. J., 1999, MNRAS, 303, 209
Marin F., 2017, A&A, 607, A40
Marin F., 2018, A&A, preprint (arXiv:1805.09098)
Marin F., Dovčiak M., Muleri F., Kislat F. F., Krawczynski H. S., 2018, MNRAS, 473, 1286
Marin F., Goosmann R. W., Gaskell C. M., 2015, A&A, 577, A66
Marin F., Goosmann R. W., Gaskell C. M., Porquet D., Dovčiak M., 2012, A&A, 548, A121
Marin F., Goosmann R. W., Petrucci P.-O., 2016, A&A, 591, A23
Marin F., Rohatgi A., Charlot S., in Reylé C., Di Matteo P., Herpin F., Lagadec E., Lançon A., Meliani Z., Royer F., eds, 2017, SF2A-2017: Proceedings of the Annual meeting of the French Society of Astronomy and Astrophysics, p .113
Marin F., Weisskopf M. C., 2017, in Reylé C., Di Matteo P., Herpin F., Lagadec E., Lançon A., Meliani Z., Royer F., eds, SF2A-2017: Proceedings of the Annual meeting of the French Society of Astronomy and Astrophysics, p. 173
Marinucci A. et al., 2016, MNRAS, 456, L94
Martin P. G., Thompson I. B., Maza J., Angel J. R. P., 1983, ApJ, 266, 470
Mason R. E., Wright G. S., Adamson A., Pendleton Y., 2007, ApJ, 656, 798
McLean I. S., Aspin C., Heathcote S. R., McCaughrean M. J., 1983, Nature, 304, 609
McNamara A. L., Kuncic Z., Wu K., 2009, MNRAS, 395, 1507
Miller G. E., Scalo J. M., 1979, ApJS, 41, 513
Miller J. S., Antonucci R. R. J., 1983, ApJ, 271, L7
Moran E. C., Barth A. J., Kay L. E., Filippenko A. V., 2000, ApJ, 540, L73
Murayama T., Taniguchi Y., 1997, PASJ, 49, L13
Muxlow T. W. B., Pedlar A., Holloway A. J., Gallimore J. F., Antonucci R. R. J., 1996, MNRAS, 278, 854
Nikulin N. S., Kuvshinov V. M., Severny A. B., 1971, ApJ, 170, L53
Packham C., Young S., Hough J. H., Axon D. J., Bailey J. A., 1997, MNRAS, 288, 375
Packham C. et al., 2007, ApJ, 661, L29
Pineault S., 1977, MNRAS, 179, 691
Prieto M. A., Reunanen J., Tristram K. R. W., Neumayer N., Fernandez-Ontiveros J. A., Orienti M., Meisenheimer K., 2010, MNRAS, 402, 724
Prunet S., Sethi S. K., Bouchet F. R., Miville-Deschenes M.-A., 1998, A&A, 339, 187
Raban D., Jaffe W., Röttgering H., Meisenheimer K., Tristram K. R. W., 2009, MNRAS, 394, 1325
Ramos Almeida C., Martínez González M. J., Asensio Ramos A., Acosta-Pulido J. A., Hönig S. F., Alonso-Herrero A., Tadhunter C. N., González-Martín O., 2016, MNRAS, 461, 1387
Rojas Lobos P. A., Goosmann R. W., Marin F., Savić D., 2018, A&A, 611, A39
Romeo A. B., Fathi K., 2016, MNRAS, 460, 2360
Sanders D. B., Phinney E. S., Neugebauer G., Soifer B. T., Matthews K., 1989, ApJ, 347, 29
Sazonov V. N., 1969, SvA, 13, 396
Scarrott S. M., Rolph C. D., Wolstencroft R. W., Tadhunter C. N., 1991, MNRAS, 249, 16P
Schartmann M., Burkert A., Krause M., Camenzind M., Meisenheimer K., Davies R. I., 2010, MNRAS, 403, 1801
Schartmann M., Meisenheimer K., Klahr H., Camenzind M., Wolf S., Henning Th., 2009, MNRAS, 393, 759
Schmitt H. R., Kinney A. L., 1996, ApJ, 463, 498
Schnittman J. D., Krolik J. H., 2009, ApJ, 701, 1175
Schnittman J. D., Krolik J. H., 2010, ApJ, 712, 908
Shakura N. I., Sunyaev R. A., 1973, A&A, 24, 337
Siebenmorgen R., Krügel E., 2007, A&A, 461, 445
Simmons J. F. L., Audit E., 2000, MNRAS, 319, 497
Simpson J. P., Colgan S. W. J., Erickson E. F., Hines D. C., Schultz A. S. B., Trammell S. R., 2002, ApJ, 574, 95
Smith J. E., Young S., Robinson A., Corbett E. A., Giannuzzo M. E., Axon D. J., Hough J. H., 2002, MNRAS, 335, 773
Sánchez-Portal M., Díaz Á. I., Terlevich E., Terlevich R., 2004, MNRAS, 350, 1087

Thronson H. A., Jr et al., 1989, ApJ, 343, 158
Thum C., Agudo I., Molina S. N., Casadio C., Gómez J. L., Morris D., Ramakrishnan V., Sievers A., 2018, MNRAS, 473, 2506
Tran H. D., 1995, ApJ, 440, 565
Tran H. D., 2003, ApJ, 583, 632
Urry C. M., Padovani P., 1995, PASP, 107, 803
Visvanathan N., Oke J. B., 1968, ApJ, 152, L165
Vollmer B., Beckert T., Davies R. I., 2008, A&A, 491, 441
Walker M. F., 1964, AJ, 69, 744
Watanabe M., Nagata T., Sato S., Nakaya H., Hough J. H., 2003, ApJ, 591, 714
Weisskopf M. C. et al., 2016, Proc. SPIE Conf. Ser. Vol. 9905, SPIE Astronomical Telescopes and Instrumentation, SPIE, Bellingham, p. 990517
Westfold K. C., 1959, ApJ, 130, 241
Wilkes B., 2004, AGN Phys. Sloan Digital Sky Survey, 311, 37
Wilson A. S., Elvis M., 1997, Ap&SS, 248, 141
Wilson A. S., Ulvestad J. S., 1982, ApJ, 263, 576
Wilson A. S., Ulvestad J. S., 1983, ApJ, 275, 8
Young S., 2000, MNRAS, 312, 567
Young S., Hough J. H., Axon D. J., Bailey J. A., Ward M. J., 1995, MNRAS, 272, 513
Zhang S. N. et al., 2016, Proc. SPIE Conf. Ser. Vol. 9905, SPIE Astronomical Telescopes and Instrumentation, SPIE, Bellingham, p. 99051Q

This paper has been typeset from a TEX/LATEX file prepared by the author.